Accepted Manuscript

Chemical and structural characterization of char development during lignocellulosic biomass pyrolysis

Lihle D. Mafu, Hein W.J.P. Neomagus, Raymond C. Everson, Christien A. Strydom, Marion Carrier, Gregory N. Okolo, John R. Bunt

Please cite this article as: Mafu, L.D., Neomagus, H.W.J., Everson, R.C., Strydom, C.A., Carrier, M., Okolo, G.N., Bunt, J.R., Chemical and structural characterization of char development during lignocellulosic biomass pyrolysis, *Bioresource Technology* (2017), doi: http://dx.doi.org/10.1016/j.biortech.2017.07.017

1 **Chemical and structural characterization of char development during lignocellulosic**

2 **biomass pyrolysis**

3 **Lihle D. Mafu[a], Hein W.J.P. Neomagus[a,b,‡], Raymond C. Everson[a,b], Christien A.**

4 **Strydom[a] Marion Carrier[c], Gregory N. Okolo[b] and John R. Bunt[b]**

5 [a]*Chemical Resource Beneficiation (CRB), School of Physical and Chemical Sciences, North-*

6 *West University, Potchefstroom Campus, Private Bag X6001 Potchefstroom, 2520, South*

7 *Africa*

8 [b]*School of Chemical and Minerals Engineering, Private Bag X6001, North-West University,*

9 *Potchefstroom Campus, Potchefstroom 2520, South Africa*

10 [c]*Aston University, EBRI, Bioenergy Research Group, Birmingham B4 7ET, United Kingdom*

11 [‡]*hein.neomagus@nwu.ac.za*

12

13 **Abstract**

14 The chemical and structural changes of three lignocellulosic biomass samples during

15 pyrolysis were investigated using both conventional and advanced characterization

16 techniques. The use of ATR-FTIR as a characterization tool is extended by the proposal of a

17 method to determine aromaticity, the calculation of both CH_2/CH_3 ratio and the degree of

18 aromatic ring condensation ($(R/C)_u$). With increasing temperature, the H/C and O/C ratios,

19 X_A and CH_2/CH_3 ratio decreased, while $(R/C)_u$ and aromaticity increased. The micropore

20 network developed with increasing temperature, until the coalescence of pores at 1100 °C,

21 which can be linked to increasing carbon densification, extent of aromatization and/or

22 graphitization of the biomass chars. WAXRD-CFA measurements indicated the gradual

23 formation of nearly parallel basic structural units with increasing carbonization temperature.

24 The char development can be considered to occur in two steps: elimination of aliphatic

25 compounds at low temperatures, and hydrogen abstraction and aromatic ring condensation at

26 high temperatures.

28

1 Introduction

Interest in the use of biomass for energy generation has grown considerably in recent years, since it is considered to be a more sustainable alternative to fossil fuels (Mao et al., 2015; Pimenidou and Dupont, 2012). One process of ensuring the efficient use of biomass in energy production is pyrolysis, where fast pyrolysis is often preferred for liquid products and low heating rates are used for the production of chars (Fisher et al., 2012). The biomass origin and the pyrolysis conditions such as heating rate, pyrolysis temperature and gas environment shape the chemical and structural characteristics of the formed chars (Rutherford et al., 2012; Wei et al., 2011). The transformation of a broad range of plant biomass sources resulted in the production of carbonaceous material displaying properties suitable for various applications such as soil amendment, gasification and co-gasification with coal (Angin and Sensoz, 2014; Kaudal et al., 2016). In addition to variable lignocellulosic composition, the presence of inorganic compounds results in peculiar reactivity of plant biomass during pyrolysis, gasification and combustion. For example, feedstocks with a high mineral matter content may be preferred for co-gasification applications due to a favourable catalytic effect of the specific minerals (Huang et al., 2009). On the other hand, low ash feedstocks may be directly transformed into liquids that should result in more stable biofuels (Antonio et al., 2014).

The intended application of pyrolytic chars is dependent on their structural and chemical characteristics, which is in turn reliant on the pyrolysis conditions. For instance, chars produced at higher temperatures have shown higher fixed carbon and elemental carbon, lower volatile matter, lower elemental oxygen and hydrogen contents (Uzun et al., 2006; Zhang et al., 2016). A number of advanced techniques has been developed and used to provide more information on the changes in characteristics induced by pyrolysis (Rutherford et al., 2012; Suliman et al., 2016). Wide angle X-ray diffraction – carbon fraction analysis (WA-XRD-CFA) has been useful in identifying the phases of biomass and has been extended to evaluating the microcrystalline parameters (Huang et al., 2009). This has been done by the determination of the interlayer spacing (d_{002}), crystalline height (L_c), crystalline diameter (L_a) and the average number of aromatic layers per carbon crystallite (N_{ave}) using the Bragg's and Scherrer's equation (Okolo et al., 2015). The transformation of the surface functionalities, or functional groups, as biomass undergoes heat treatment, has been studied by Fourier Transforms infrared (FTIR) spectroscopy. Major findings include the elimination of aliphatic groups at lower temperatures and as heating temperatures were increased, the aromatic

2

62　functional groups lost their infrared activity resulting in a spectrum with no FTIR peaks

63　(Rutherford et al., 2012; Suliman et al., 2016). Cui et al. (2016) used FTIR to extract coal

64　structural parameters which included the fraction of aromatic and aliphatic fractions. It was

65　concluded that the CH_2/CH_3 ratio increased with coal rank, pyrolysis temperature and

66　pyrolysis time. Most findings from FTIR have been complemented by results from cross

67　polarization magnetic angle spinning nuclear magnetic resonance (CPMAS ^{13}C NMR)

68　spectroscopy and surface area measurements (McBeath et al., 2011; Suliman et al., 2016).

69　In addition, the characterization techniques have revealed important details in the process of

70　char formation, which depends on the pyrolysis conditions and biomass characteristics. The

71　lignocellulosic fibre composition has been reported to be the basis of observed chemical and

72　structural changes during low temperature pyrolysis (Mafu et al., 2016; Wannapeera and

73　Worasuwannarak, 2012). At temperatures above 500 °C, the vast majority of fibres have been

74　found to be consumed through decomposition.

75　When considering processing conditions in a typical fixed bed dry bottom (FBDB) gasifier,

76　the pyrolysis zone may rise up to temperatures above 1000 °C, while the heating rate is

77　relatively low (10 – 20 °C/min) (Skhonde et al., 2009) and as such, the understanding of slow

78　pyrolysis char formation even up to higher temperatures is justified. The characteristics of

79　chars produced from the pyrolysis zone affect the gasification kinetics during biomass

80　gasification or co-gasification with coal (Kajitani et al., 2010; Y. Zhang et al., 2016). It has

81　been reported that the aromaticity, for instance, is a function of charring temperature

82　(Everson et al., 2013), which increases with increasing pyrolysis temperature, while the

83　gasification reactivity of the formed char has been shown to decrease with increasing

84　aromaticity. However, as aromatization progresses, other chemical transformations that affect

85　the crystallinity, the surface area and the microcrystalline structure are simultaneously taking

86　place. The progress of char formation in slow pyrolysis, together with correlations between

87　the various char characteristics have not yet received significant attention, and forms the

88　motivation of this study.

89　The chemical and structural characterization of biomass, similar to coal, provides insight in

90　the thermal behaviour, such as the gasification reactivity. As such, this work reports on the

91　slow pyrolysis char development in the region of torrefaction to gasification temperatures.

92　The effect of temperature on three different biomass samples that are widely available in

93　South Africa is discussed, and outcomes include: the determination of aromaticity (f_{aF}),

94　degree of aromatic ring condensation (($R/C)_u$), and aliphatic CH_2/CH_3 ratios from ATR-FTIR

3

95 spectroscopy data; fraction of amorphous carbon (X_A) and Van Krevelen plots of the

96 samples. From the reported results, the char development is then explained using both

97 chemical and structural characteristics by relating aromaticity to other char characteristics,

98 which has been an area that is inadequately explored in biomass studies.

99 **2   Materials and Methods**

100 **2.1   Materials**

101 Three abundantly available biomass sources in South Africa were procured. Softwood (SW)

102 and hardwood (HW) chips were supplied by South African Pulp and Paper Industries Limited

103 (SAPPI), whereas sweet sorghum bagasse (SB) was obtained from the Agricultural Research

104 Council (ARC) in Potchefstroom. Approximately 10 kg of each sample was obtained and air-

105 dried overnight. Successively, the sample size was representatively reduced by applying a

106 standardised cone and quartering method (DD CEN/TS 14780:2005) three times. The

107 obtained sample was ground to < 300 μm and was further used for characterisation and

108 conversion experiments. From the bulk samples, about 15 g of the air-dried and ground

109 biomass samples were heated at 10 °C/min using a N_2 gas flow rate of 100 ml/min from room

110 temperature to 260 °C in a tube furnace from Elite Thermal Systems Limited (Model

111 TSH12/75/610) to achieve a 30% mass loss. The changes in characteristics after torrefaction

112 are reported in a previous study (Mafu et al., 2016). Chars for this study were prepared from

113 the torrefied biomass, in the same furnace by heating at 10 °C/min to final temperatures of

114 300, 400, 600 and 1100 °C and left isothermal for 60 minutes. The series of pyrolytic chars

115 were referred to by the plant biomass that they were produced from, and the highest

116 temperature of the pyrolysis treatment (e.g. softwood char prepared at 300 °C is referred to as

117 SW 300).

118 **2.2   Characterization**

119 Ultimate analysis was carried out by means of the standard ASTM D 5373 method for

120 elemental C, H and N, whilst the elemental S and O mass percentages were determined by the

121 ASTM D 4239 method and by difference, respectively. The volatile matter and mineral

122 matter contents were obtained using the ISO 562:2010 and ISO 1171:2010 methods

123 respectively, whilst the fixed carbon content was calculated by difference. Both analyses

124 were carried out by the Council of Geosciences, Pretoria, South Africa. Infrared spectra were

125 recorded using a Perkin–Elmer Paragon 1000 PC Fourier Transforms Infrared (FTIR)

126 spectrometer with an attenuated total reflectance (ATR) accessory between 400 and 4000 cm⁻

127   [1] with 4 cm^{-1} resolution, where 32 scans were averaged for one sample run. CPMAS ^{13}C

128   NMR experiments were carried out at the Central Analytical Facility of Stellenbosch

129   University following the method by Melkior et al. (2012), which involves a combination of

130   cross polarization and magnetic angle spinning techniques. A Quanta FEG 250

131   Environmental Scanning electron microscope (ESEM) under an acceleration voltage of 30

132   kV was used to capture the surface morphology of biomass char samples and the imaging

133   was improved by lightly covering the sample with a gold layer at the Laboratory of Electron

134   Microscopy (LEM) of the North-West University. WA-XRD-CFA was conducted at the

135   North-West University following a method outlined in Mafu et al. (2016). Surface area

136   measurements were obtained from a Micrometrics ASAP 2020 surface area and porosity

137   analyser. Samples were degassed under vacuum, at 75 °C for 48 h and analysis conducted at

138   0 °C at a relative pressure range: $0 < P/P_0 \leq 0.032$: where P is the analysis pressure and P_0 is

139   the saturation vapour pressure of CO_2. The Dubinin-Radushkevich (D-R) and Horvath-

140   Kawazoe (H-K) models were used to obtain the micropore surface area, maximum pore

141   volume and median pore width (Okolo et al., 2015).

142   From ATR-FTIR spectroscopy, the sum of aromatic functional groups and the sum of

143   aliphatic functional groups, derived by Gaussian curve deconvolution, were used to calculate

144   the aromaticity. The aromaticity ($f_{a,F}$), defined as the fraction of aromatic groups from the

145   sum of aliphatic and aromatic groups in the sample is given by Equation 1. The aromaticity

146   values from this proposed method were compared to those determined from CPMAS ^{13}C

147   NMR ($f_{a,N}$). The $f_{a,F}$ was then used to calculate the degree of aromatic ring condensation

148   (Equation 2) which was found to be proportional to the total aromaticity ($f_{a,F}$ in this case) and

149   the fraction of aromatic hydrogen (H_{ar}) to aromatic carbon (C_{ar}) by Cui et al., (2016). The

150   asymmetric stretching of CH_3 and CH_2 groups have been used as an indication of the degree

151   of cyclization, where a higher value of CH_2/CH_3 revealed longer aliphatic chains or a higher

152   degree of cyclization. The value of CH_2/CH_3 was determined using Equation 3 where A_{2925}

153   and A_{2955} represent the area under the deconvoluted curves of ATR-FTIR peaks at 2925 and

154   2955 cm^{-1}, respectively. The fraction of amorphous carbon, X_A, was determined by the

155   Gaussian curve deconvolution of the amorphous and crystalline phases of the 002 band of the

156   XRD spectra (Figure 1). The area under the curve at position 16° and 25° after deconvolution

157   were assigned to the amount of amorphous carbon (S_A) and crystalline carbon (S_C),

158   respectively. X_A was calculated using Equation 4 (Okolo et al., 2015). Using the empirical

159   Bragg's and Scherrer's equations, the crystallite height (L_c), crystallite diameter (L_a),

5

160 interlayer spacing (d_{002}) and average number of aromatic layers per carbon crystallite (N_{ave})

161 were calculated (Everson et al., 2013; Okolo et al., 2015).

162
$$f_{aF} = \frac{\sum C_{ar}}{\sum C_{ar+al}} \tag{1}$$

163
$$\left(\frac{R}{C}\right)_u = 1 - \frac{1}{2}\left(f_a + \frac{H_{ar}}{C_{ar}}\right) \tag{2}$$

164
$$\frac{CH_2}{CH_3} = \frac{A_{2925/cm}}{A_{2955/cm}} \tag{3}$$

165
$$X_A = \frac{S_A}{S_A + S_C} \tag{4}$$

166 **3   Results and discussion**

167 **3.1   Chemical characteristics**

168 Table 1 presents the chemical characteristics of the pyrolytic chars. Char development

169 progressed with increasing temperature through the evolution of volatiles, which results in

170 increased fixed carbon and mineral matter contents. The proximate analyses showed minor

171 changes between torrefied biomass and chars prepared at 300 °C. Further changes up to 600

172 °C were linked to the decomposition of cellulose and lignin (Giudicianni et al., 2013). The

173 differences in proximate analyses chars prepared at 600 and 1100 °C were significant and

174 reported to be mainly driven by secondary reactions (Anca-Couce, 2016). The calorific value

175 (CV) increased with increasing pyrolysis temperature, but decreased at 1100 °C for all

176 biomass samples. The increase in CV at lower temperatures is attributed to the reduction in

177 elemental O and H, and increasing carbon content (carbon densification) in the solid matrix.

178 However, the graphitization of the solid mass at high temperatures accounts for the reduction

179 in CV for the for the 1100 °C chars, as observed for coal (Suggate and Dickinson, 2004).

180 Increasing pyrolysis temperature resulted in the increase in elemental carbon, whilst

181 elemental oxygen and hydrogen decreased appreciably. Noteworthy were the larger changes

182 in ultimate analysis results from torrefied biomass to chars prepared at 600 °C as a result of

183 the degradation of lignocellulosic fibres (Yang et al., 2006). Beyond 600 °C, changes were a

184 result of bond reordering and hydrogen abstraction as shown by further decreases in

185 elemental H and O (Trubetskaya et al., 2016a). The amounts of N and S were very low; as

6

186 such no trends could be drawn. The changes in C, H and O amounts result in the reduction of

187 the H/C and O/C ratios linked to an increase in aromaticity (Anupam et al., 2016). The

188 decrease of H/C and O/C ratios as shown in the Van Krevelen plot (Figure 2) with

189 temperature was comparable to the coalification process with torrefied biomass' ratios similar

190 to those of peat and chars prepared at 1100 °C to anthracite coals (Anupam et al., 2016;

191 Suggate and Dickinson, 2004).

192 ATR-FTIR spectra for chars prepared at 1100 °C could not be collected due to line

193 broadening and absence of vibrating and stretching functional groups at high temperatures

194 (Roberts et al., 2015; Rutherford et al., 2012). Torrefied biomass displayed characteristic

195 vibrations corresponding to the presence of aliphatic groups (3200-3500, 2800-3000 and 900-

196 1150 cm^{-1}) and aromatic groups (700-900, 1150-1650 cm^{-1}) (Huang et al., 2015; Zhao et al.,

197 2013) which can be attributed to the presence of residual lignocellulosic fibres (Anca-Couce,

198 2016; Pimenidou and Dupont, 2012).

199 The deconvoluted area under the aromatic ATR-FTIR peaks could not be related to the

200 amounts of lignin at torrefaction conditions (Mafu et al., 2016), but from both aliphatic and

201 aromatic peaks, the aromaticity of the materials could be determined. SB had the lowest

202 aromaticity of the torrefied biomass samples, due to the lower lignin contents in the parent

203 biomass, compared to SW and HW (Mafu et al., 2016). Aromaticity increased with

204 increasing pyrolysis temperature (Table 2) as alluded to previously by other researchers

205 (Asadullah et al., 2010; McBeath et al., 2011). The observed increase in aromaticity had two

206 contributing factors: (1) the elimination of aliphatic groups taking place more rapidly than the

207 loss of aromatics and (2) the condensation of aromatic rings as observed by the increase in

208 $(R/C)_u$ with increasing pyrolysis temperature (Table 2). The parameter, CH_2/CH_3 ratio, was

209 determined and the results are presented in Table 2. For torrefied biomass samples, the

210 CH_2/CH_3 ratio was around 50 and decreased with increasing temperature to approximately 1

211 for chars prepared at 600 °C. This could be a consequence of progressing cyclization of the

212 aliphatics, as well as the shorter $-CH_2$ aliphatic chains being easily broken compared to the

213 longer $-CH_3$ aliphatic chains (Cui et al., 2016). Functionalities containing elemental H and O

214 gradually decreased at pyrolysis temperatures up to 300 °C as a result of dehydration

215 (Rutherford et al., 2012). Subsequent elimination of aliphatic functionalities, H- and O-

216 containing functional groups up to 600 °C could be related to the degradation of fibre

217 components (Yang et al., 2013) and was consistent with the ultimate analysis data (Table 1).

218 From CPMAS ^{13}C NMR spectroscopy, the presence of acetyl, methoxyl, amorphous and

219 crystalline carbons of cellulose and aromatic groups of lignin in all biomass samples could be

220 confirmed by the presence of peaks at characteristic positions (Freitas et al., 2001; Mafu et

221 al., 2016). For chars prepared at 300 °C, peaks related to hemicelluloses and amorphous

222 carbons of cellulose and lignin, gradually decreased as a result of the degradation of the

223 lignocellulosic fibres. Peaks at 35, 68, 62, 65, 73, 84, 105, 112 and 149 ppm were visible for

224 chars at 300 °C and related to the carbons of the crystalline cellulose and lignin (Bardet et al.,

225 2007; Melkior et al., 2012). Shoulder peaks at 62-65 ppm and 72-74 ppm were as a result of

226 residual amorphous carbons (Mafu et al., 2016). At 400 °C, the peak areas of characteristic

227 cellulose and lignin peaks reduced, as a result of the reduction of their carbon functionalities

228 (Rutherford et al., 2012). Chars prepared at 600 °C had mainly aromatic carbon

229 functionalities with fractions of amorphous C=C and C-H left in the chars. The differences

230 between woody biomass and SB were more significant for chars prepared at 300 °C, and

231 converged to almost the same ^{13}C chemical structure at 600 °C, which was also observed by

232 McBeath et al., (2011) for different lignocellulosic biomass samples. These findings suggests

233 that char development may be broadly defined as a two-step process, where the first step (<

234 600 °C) is accompanied by lignocellulosic fibre degradation linked to the net loss of the

235 aliphatic fraction of biomass. The second step (> 600 °C) may be assigned to the

236 reorganisation of bonds that result in the conjugation of aromatic bonds, hence increasing

237 further, the aromaticity of chars. The aromaticity as determined through both ATR-FTIR and

238 NMR were comparable as presented in Table 2.

239 **3.2   Structural characteristics**

240 Due to the insignificant changes as pyrolysis temperatures were increased to 1100 °C, only

241 torrefied, 300 and 1100 °C char micrographs are presented and discussed. The surface for all

242 torrefied biomass was smooth, possibly from the melting of lignin and cellulose (Mafu et al.,

243 2016). With increasing temperature, the matrix did not change but rather became brittle

244 (Cetin et al., 2004), that is, the escape of volatiles left a rigid, hollow biomass matrix

245 (Trubetskaya et al., 2016a). A slight broadening of the water conducting pores was also

246 observed for all biomass samples with increasing pyrolysis temperature (Liu et al., 2010;

247 Trubetskaya et al., 2016a).

248 The diffractograms showed two broad and distinct peaks at the 2θ positions 16 and 25°

249 assigned to amorphous and graphitic basal planes, respectively. Most of the crystalline carbon

250 in biomass is in general ascribed to the presence of cellulose, whilst the other lignocellulosic

8

251   fibres contribute to the amorphous carbon content (Barnette et al., 2012; Murillo et al., 2014).

252   The intensities of both peaks were lesser for SB than HW and SW, which was a direct

253   consequence of the higher amount of mineral matter and lower content in original

254   lignocellulosic fibres in SB than HW and SW (Mafu et al., 2016). As the pyrolysis

255   temperature increased, the amorphous carbon peak (16°) progressively disappeared, in line

256   with the degradation of hemicelluloses and other amorphous fractions of biomass. The

257   crystalline phase narrowed as the temperature increased from 300 to 600 °C, following the

258   degradation of celluloses at these conditions (Tumuluru et al., 2011; Yang et al., 2007). Chars

259   prepared at 1100 °C showed increased peak intensity at 27° which may be a result of the

260   recrystallization of some of the carbon material in the matrix (Azargohar et al., 2014).

261   Increasing pyrolysis temperature promoted structural orderliness within the residual solid

262   matrix as illustrated by the shift of the (002) band towards higher angle (2θ) regions (25 –

263   28°). The emergence of sharp peaks at 52 and 60° reflected the increasing share of minerals

264   such as oxides and carbonates of Si, Mg and Ca (Trubetskaya et al., 2016b; Wen et al., 2014).

265   CO_2 adsorption results showed an increase in the micropore surface area with increasing

266   pyrolysis temperature up to 600 °C (Table 3). This occurred through the development of

267   micropores, with increasing micropore volume as volatiles were increasingly driven off,

268   facilitated by carbon densification in the bulk biomass char. At 1100 °C, both micropore

269   surface area and micropore volumes decreased for SW and SB. This was ascribed to pore

270   coalescence at higher temperatures (Angin and Sensoz, 2014; Mukome et al., 2013).

271   Pyrolytic chars prepared from HW at 1100 °C were an exception as they demonstrated an

272   increase in the surface area and pore volume (Table 3). This could be a consequence of the

273   accumulation of pores in the higher micropore range without a disruption of the lower

274   micropore range, which was not the case for SB and SW. The lower pore volumes, and

275   consequently surface areas of SB compared those of the woody biomass samples may be as a

276   result of the higher ash values which may hinder pore development and/or block the access of

277   pores by CO_2 (Tumuluru et al., 2011). There were no significant changes in the average pore

278   diameter as the pyrolysis temperature increased. They ranged from 3.5-4.1 Å for all biomass

279   samples suggesting that pore development happens through the formation of channels with

280   deeper pores (Mafu et al., 2016).

281   The structural lattice parameters and fraction of amorphous carbon, X_A, are presented in

282   Table 3. The different torrefied biomass samples showed approximately the same amounts

283   (fractions) of amorphous carbon. The determined X_A was reported as being representative of

284   the amorphous sections of the fibres, which were not degraded during heat treatment (Mafu et

285   al., 2016). Pyrolytic chars of SB were more sensitive to heat owing to the limited shielding by

286   the lower lignin contents in SB compared to HW and SW. At 600 °C, X_A could not be

287   determined by means of WA-XRD-CFA for SB char, while this was observed only at 1100

288   °C for HW and SW chars. As the pyrolysis temperature increased, d_{002}, L_c and N_{ave} decreased

289   significantly, whilst L_a was considerably increased. The reduction in d_{002} resulted in the

290   decrease of L_c producing a more packed microcrystallite lattice. Thus, the carbon crystallite

291   of the biomass chars were significantly stretched in the y-direction resulting in flat layered

292   carbon sheets. The average number of crystallites in a stack was reduced as d_{002} and L_c

293   decreased. These lattice parameter changes may indicate changes of the micropore network.

294   From 600 °C, the structural parameters of woody biomass became more similar to each other

295   and increasingly different from that of the bagasse sample. This may be a consequence of the

296   rearrangement reactions that dominate char formation at high temperatures (Trubetskaya et

297   al., 2016a).

298   The extracted characteristics of biomass and subsequent chars were correlated with their H/C

299   ratios as presented in Figure 3 (a – c). Inverse linear correlations were observed between the

300   H/C ratios and the aromaticity (Figure 3(a)), and the degree of aromatic ring condensation,

301    $(R/C)_u$, of the chars as shown in Figure 3(b). This implies that both the aromaticity and $(R/C)_u$

302   can be predicted from the empirical H/C ratios, following the correlation equations shown in

303   Table 4, with correlation coefficients > 0.98. Conversely, the CH_2/CH_3 ratio was found to

304   increase with increasing H/C ratio (equivalent to decreasing aromaticity) as presented in

305   Figure 3(c) with a power law fitting. It has been demonstrated that the CH_2/CH_3 ratios of the

306   chars can as well, be estimated from the H/C ratios of the studied samples from the

307   correlation equations given in Table 4. Thus, with increasing pyrolysis temperature, char

308   development proceeds by the elimination of aliphatic groups while aromaticity increases,

309   complemented by the progression of aromatic ring condensation, $(R/C)_u$, with the

310   concomitant hydrogen abstraction. These processes, coupled with increasing carbon

311   densification of the biomass chars, also impacted the pore structure evolution and

312   development. For example, the micropore surface area as shown in Figure 6(d) and the

313   micropore volume (Table 3) increased with increasing with increasing pyrolysis temperature

314   up to 600 °C. This may be linked to the elimination of aliphatic chains and the escape of

315   volatiles leaving behind pores as the pyrolysis temperature increased. However, pore

316   coalescence was observed for char samples of SW and SB at 1100 °C, similar to reported

10

317 findings for coal (Roberts et al., 2015). From these established correlations, it is evident that

318 the charring process is a combination of aliphatics elimination and the aromatic ring

319 condensation which results in the gradual increase in aromaticity with increasing temperature.

320 **4   Conclusions**

321 Char development was found to be dependent on the pyrolysis conditions. There was an

322 observed link between the proximate and ultimate analysis data with fibre degradation.

323 Chemical properties of the chars can be extracted from ATR-FTIR data, complimenting

324 results from other techniques. Gradual decrease in H/C and O/C ratios, and aliphatic chains

325 with increasing pyrolysis temperature, resulted in increasing f_a and $(R/C)_u$ of the chars. While

326 micropore development was observed up to 600 °C, pore coalescence was more significant

327 for SW and SB at 1100 °C. Char development can be considered as a two steps process: <

328 600 °C where changes were attributed to fibre degradation, resulting in the removal of

329 aliphatics, and > 600 °C where changes were as a result of hydrogen abstraction and aromatic

330 ring condensation.

331 **Acknowledgments**

338 **Appendix A**

339 Supplementary data associated with this article can be found, in the online version, at

340 **References**

341   1. Anca-Couce, A., 2016. Reaction mechanisms and multi-scale modelling of
342   lignocellulosic biomass pyrolysis. Prog. Energy Combust. Sci. 53, 41–79.

343   2. Angin, D., Sensoz, S., 2014. Effect of Pyrolysis Temperature on Chemical and
344   Surface Properties of Biochar of Rapeseed (*Brassica napus L.*). Int. J.
345   Phytoremediation 16, 684–693.

346   3. Antonio, W., Lenço, P.C., Carvalho, D.J., Paulo, J., Veiga, S., 2014. The generation
347   of residual biomass during the production of bio-ethanol from sugarcane , its
348   characterization and its use in energy production. Renew. Sustain. Energy Rev. 29,

349   589–603.

350   4. Anupam, K., Sharma, A.K., Lal, P.S., Dutta, S., Maity, S., 2016. Preparation,
351   characterization and optimization for upgrading *Leucaena leucocephala* bark to
352   biochar fuel with high energy yielding. Energy 106, 743–756.

353   5. Asadullah, M., Zhang, S., Min, Z., Yimsiri, P., Li, C.-Z., 2010. Effects of biomass
354   char structure on its gasification reactivity. Bioresour. Technol. 101, 7935–43.

355   6. Azargohar, R., Nanda, S., Kozinski, J.A., Dalai, A.K., Sutarto, R., 2014. Effects of
356   temperature on the physicochemical characteristics of fast pyrolysis bio-chars derived
357   from Canadian waste biomass. Fuel 125, 90–100.

358   7. Bardet, M., Hediger, S., Gerbaud, G., Gambarelli, S., Jacquot, J.F., Foray, M.F., 2007.
359   Investigation with ^{13}C NMR , EPR and magnetic susceptibility measurements of char
360   residues obtained by pyrolysis of biomass. Fuel 86, 1966–1976.

361   8. Barnette, A.L., Lee, C., Bradley, L.C., Schreiner, E.P., Bum, Y., Shin, H., Cosgrove,
362   D.J., Park, S., Kim, S.H., 2012. Quantification of crystalline cellulose in
363   lignocellulosic biomass using sum frequency generation (SFG) vibration spectroscopy
364   and comparison with other analytical methods. Carbohydr. Polym. 89, 802–809.

365   9. Cetin, E., Moghtaderi, B., Gupta, R., Wall, T.F., 2004. Influence of pyrolysis
366   conditions on the structure and gasification reactivity of biomass chars. Fuel 83,
367   2139–2150.

368   10. Cui, T., Fan, W., Dai, Z., Guo, Q., Yu, G., Wang, F., 2016. Variation of the coal
369   chemical structure and determination of the char molecular size at the early stage of
370   rapid pyrolysis. Appl. Energy 179, 650–659.

371   11. Everson, R.C., Okolo, G.N., Neomagus, H.W.J.P., Santos, J., 2013. X-ray diffraction
372   parameters and reaction rate modeling for gasification and combustion of chars
373   derived from inertinite-rich coals. Fuel 109, 148–156.

374   12. Fisher, E.M., Dupont, C., Darvell, L.I., Commandré, J.M., Saddawi, a., Jones, J.M.,
375   Grateau, M., Nocquet, T., Salvador, S., 2012. Combustion and gasification
376   characteristics of chars from raw and torrefied biomass. Bioresour. Technol. 119,
377   157–165.

378   13. Freitas, J.C.C., Bonagamba, T.J., Emmerich, F.G., 2001. Investigation of biomass-
379   and polymer-based carbon materials using ^{13}C high-resolution solid-state NMR.
380   Carbon. 39, 535–545.

381   14. Giudicianni, P., Cardone, G., Ragucci, R., 2013. Cellulose , hemicellulose and lignin
382   slow steam pyrolysis : Thermal decomposition of biomass components mixtures. J.

12

383   Anal. Appl. Pyrolysis 100, 213–222.

384   15. Huang, L., Chen, Y., Liu, G., Li, S., Liu, Y., Gao, X., 2015. Non-isothermal pyrolysis

385   characteristics of giant reed (*Arundo donax L.*) using thermogravimetric analysis.

386   Energy 87, 31–40.

387   16. Huang, Y., Yin, X., Wu, C., Wang, C., Xie, J., Zhou, Z., Ma, L., Li, H., 2009. Effects

388   of metal catalysts on CO_2 gasification reactivity of biomass char. Biotechnol. Adv. 27,

389   568–72.

390   17. Kajitani, S., Zhang, Y., Umemoto, S., Ashizawa, M., Hara, S., 2010. Co-gasification

391   reactivity of coal and woody biomass in high-temperature. Energy & Fuels 24, 145–

392   151.

393   18. Kaudal, B.B., Chen, D., Madhavan, D.B., Downie, A., Weatherley, A., 2016. An

394   examination of physical and chemical properties of urban biochar for use as growing

395   media substrate. Biomass and Bioenergy 84, 49–58.

396   19. Liu, Z., Zhang, F., Wu, J., 2010. Characterization and application of chars produced

397   from pinewood pyrolysis and hydrothermal treatment. Fuel 89, 510–514.

398   20. Mafu, L.D., Neomagus, H.W.J.P., Everson, R.C., Carrier, M., Strydom, C.A., Bunt,

399   J.R., 2016. Structural and chemical modifications of typical South African biomasses

400   during torrefaction. Bioresour. Technol. 202, 192–197.

401   21. Mao, Y., Dong, L., Dong, Y., Liu, W., Chang, J., Yang, S., Lv, Z., Fan, P., 2015. Fast

402   co-pyrolysis of biomass and lignite in a micro fluidized bed reactor analyzer.

403   Bioresour. Technol. 181, 155–162.

404   22. McBeath, A. V, Smernik, R.J., Schneider, M.P.W., Schmidt, M.W.I., Plant, E.L.,

405   2011. Determination of the aromaticity and the degree of aromatic condensation of a

406   thermosequence of wood charcoal using NMR. Org. Geochem. 42, 1194–1202.

407   23. Melkior, T., Jacob, S., Gerbaud, G., Hediger, S., Pape, L. Le, Bonnefois, L., Bardet,

408   M., 2012. NMR analysis of the transformation of wood constituents by torrefaction.

409   Fuel 92, 271–280.

410   24. Mukome, F.N.D., Zhang, X., Silva, L.C.R., Six, J., Parikh, S.J., 2013. Use of

411   chemical and physical characteristics to investigate trends in biochar feedstocks. J.

412   Agric. Food Chem. 61, 2196–2204.

413   25. Murillo, J.D., Ware, E.A., Biernacki, J.J., 2014. Characterization of milling effects on

414   the physical and chemical nature of herbaceous biomass with comparison of fast

415   pyrolysis product distributions using Py-GC/MS. J. Anal. Appl. Pyrolysis 108, 234–

416   247.

13

417   26. Okolo, G.N., Neomagus, H.W.J.P., Everson, R.C., Roberts, M.J., Bunt, J.R.,
418   Sakurovs, R., Mathews, J.P., 2015. Chemical–structural properties of South African
419   bituminous coals: Insights from wide angle XRD–carbon fraction analysis, ATR–
420   FTIR, solid state ^{13}C NMR, and HRTEM techniques. Fuel 158, 779–792.

421   27. Pimenidou, P., Dupont, V., 2012. Characterisation of palm empty fruit bunch (PEFB)
422   and pinewood bio-oils and kinetics of their thermal degradation. Bioresour. Technol.
423   109, 198–205.

424   28. Roberts, M.J., Everson, R.C., Neomagus, H.W.J.P., Okolo, G.N., Van Niekerk, D.,
425   Mathews, J.P., 2015. The characterisation of slow-heated inertinite- and vitrinite-rich
426   coals from the South African coalfields. Fuel 158, 591–601.

427   29. Rutherford, D.W., Wershaw, R.L., Rostad, C.E., Kelly, C.N., 2012. Effect of
428   formation conditions on biochars : Compositional and structural properties of
429   cellulose , lignin , and pine biochars. Biomass and Bioenergy 46, 693–701.

430   30. Skhonde, M.P., Matjie, R.H., Bunt, J.R., Strydom, A.C., Schobert, H., 2009. Sulfur
431   Behavior in the Sasol-Lurgi Fixed-Bed Dry-Bottom Gasification process. Energy &
432   Fuels 23, 229–235.

433   31. Suggate, R.P., Dickinson, W.W., 2004. Carbon NMR of coals: The effects of coal
434   type and rank. Int. J. Coal Geol. 57, 1–22.

435   32. Suliman, W., Harsh, J.B., Abu-Lail, N.I., Fortuna, A.M., Dallmeyer, I, Garcia-Perez,
436   M., 2016. Influence of feedstock source and pyrolysis temperature on biochar bulk
437   and surface properties. Biomass and Bioenergy 84, 37–48.

438   33. Trubetskaya, A., Jensen, P.A., Jensen, A.D., Garcia Llamas, A.D., Umeki, K.,
439   Glarborg, P., 2016a. Effect of fast pyrolysis conditions on biomass solid residues at
440   high temperatures. Fuel Process. Technol. 143, 118–129.

441   34. Trubetskaya, A., Jensen, P.A., Jensen, A.D., Steibel, M., Spliethoff, H., Glarborg, P.,
442   Larsen, F.H., 2016b. Comparison of high temperature chars of wheat straw and rice
443   husk with respect to chemistry, morphology and reactivity. Biomass and Bioenergy
444   86, 76–87.

445   35. Tumuluru, J.S., Sokhansanj, S., Hess, J.R., Wright, C.T., Boardman, R.D., 2011. A
446   review on biomass torrefaction process and product properties for energy
447   applications. Ind. Biotechnol. 7, 384–402.

448   36. Uzun, B.B., Putun, A.E., Ersan, P., 2006. Fast pyrolysis of soybean cake : Product
449   yields and compositions. Bioresour. Technol. 97, 569–576.

450   37. Wannapeera, J., Worasuwannarak, N., 2012. Upgrading of woody biomass by

14

451   torrefaction under pressure. J. Anal. Appl. Pyrolysis 96, 173–180.

452   38. Wei, L., Zhang, L., Xu, S., 2011. Effects of feedstock on co-pyrolysis of biomass and

453   coal in a free-fall reactor. J. Fuel Chem. Technol. 39, 728–734.

454   39. Wen, J.-L., Sun, S.-L., Yuan, T.-Q., Xu, F., Sun, R.-C., 2014. Understanding the

455   chemical and structural transformations of lignin macromolecule during torrefaction.

456   Appl. Energy 121, 1–9.

457   40. Yang, D., Zhong, L., Yuan, T., Peng, X., Sun, R., 2013. Studies on the structural

458   characterization of lignin , hemicelluloses and cellulose fractionated by ionic liquid

459   followed by alkaline extraction from bamboo. Ind. Crop. Prod. 43, 141–149.

460   41. Yang, H., Yan, R., Chen, H., Lee, D.H., Zheng, C., 2007. Characteristics of

461   hemicellulose , cellulose and lignin pyrolysis. Fuel 86, 1781–1788.

462   42. Yang, H., Yan, R., Chen, H., Zheng, C., Lee, D.H., Uni, V., V, N.D., March, R. V,

463   Re, V., Recei, M., September, V., 2006. In-depth investigation of biomass pyrolysis

464   based on three major components : hemicellulose , cellulose and lignin. Energy and

465   Fuels 388–393.

466   43. Zhang, Y., Zheng, Y., Yang, M., Song, Y., 2016. Effect of fuel origin on synergy

467   during co-gasification of biomass and coal in CO_2. Bioresour. Technol. 200, 789–794.

468   44. Zhang, Li, L., Tong, D., Hu, C., 2016. Microwave-enhanced pyrolysis of natural algae

469   from water blooms. Bioresour. Technol. 212, 311–317.

470   45. Zhao, X., Chen, J., Chen, F., Wang, X., Zhu, Q., Ao, Q., 2013. Surface

471   characterization of corn stalk superfine powder studied by FTIR and XRD. Colloids

472   Surfaces B Biointerfaces 104, 207–212.

473

474

15

475 **Figure captions**

476 **Figure 1:** Determination of X_A by Gaussian curve deconvolution of the (002) band for SB

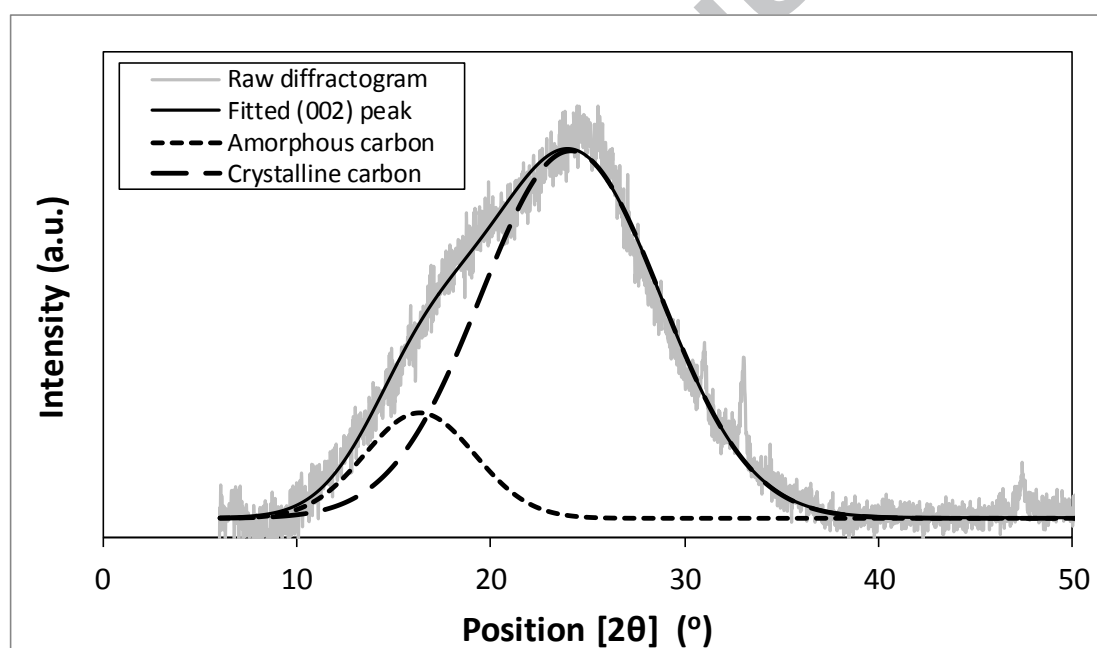477 char prepared at 300 °C.

478 **Figure 2.** Comparison of the coalification process with biomass char formation in a Van

479 Krevelen Plot.

480 **Figure 3:** Correlations between the chemical characteristics of biomass and biomass chars.
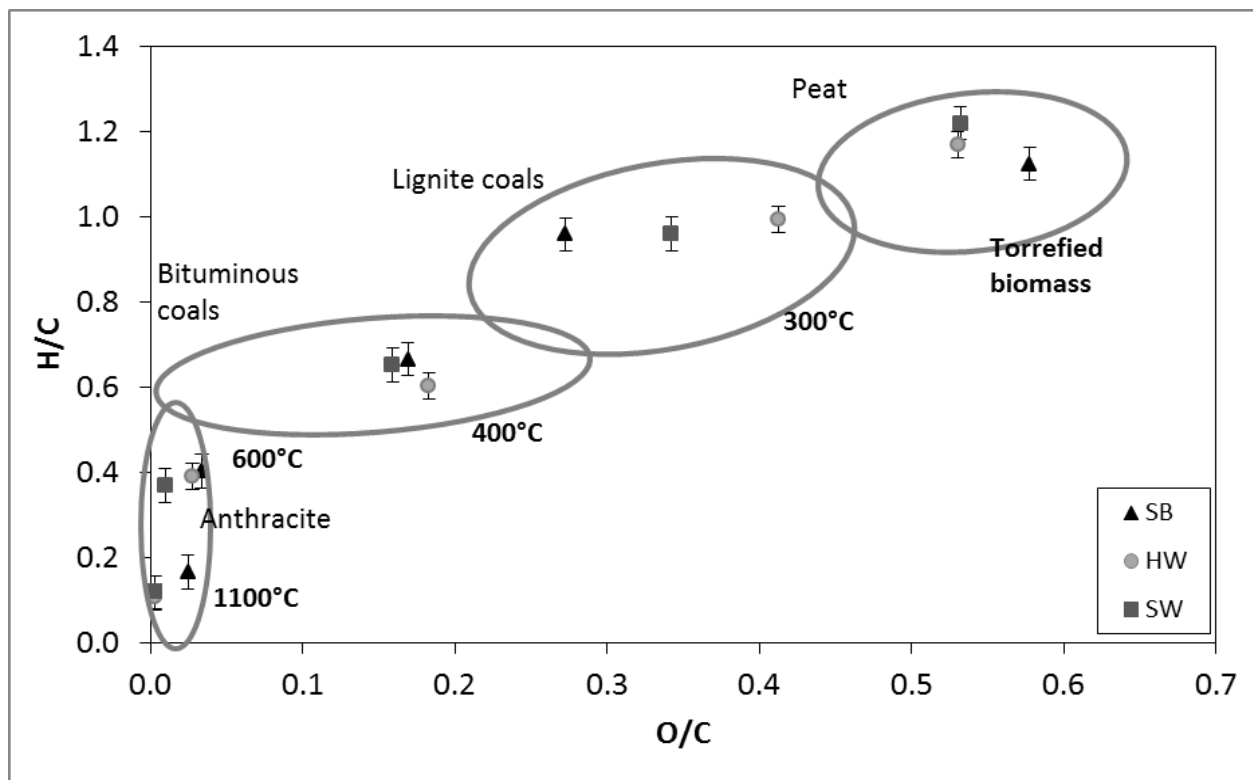
481

482

483

484

485 **Figure 1:** Determination of X_A by Gaussian curve deconvolution of the (002) band for SB
486 char prepared at 300 °C.

487

488

16

Figure 2. Comparison of the coalification process with biomass char formation in a Van Krevelen Plot.
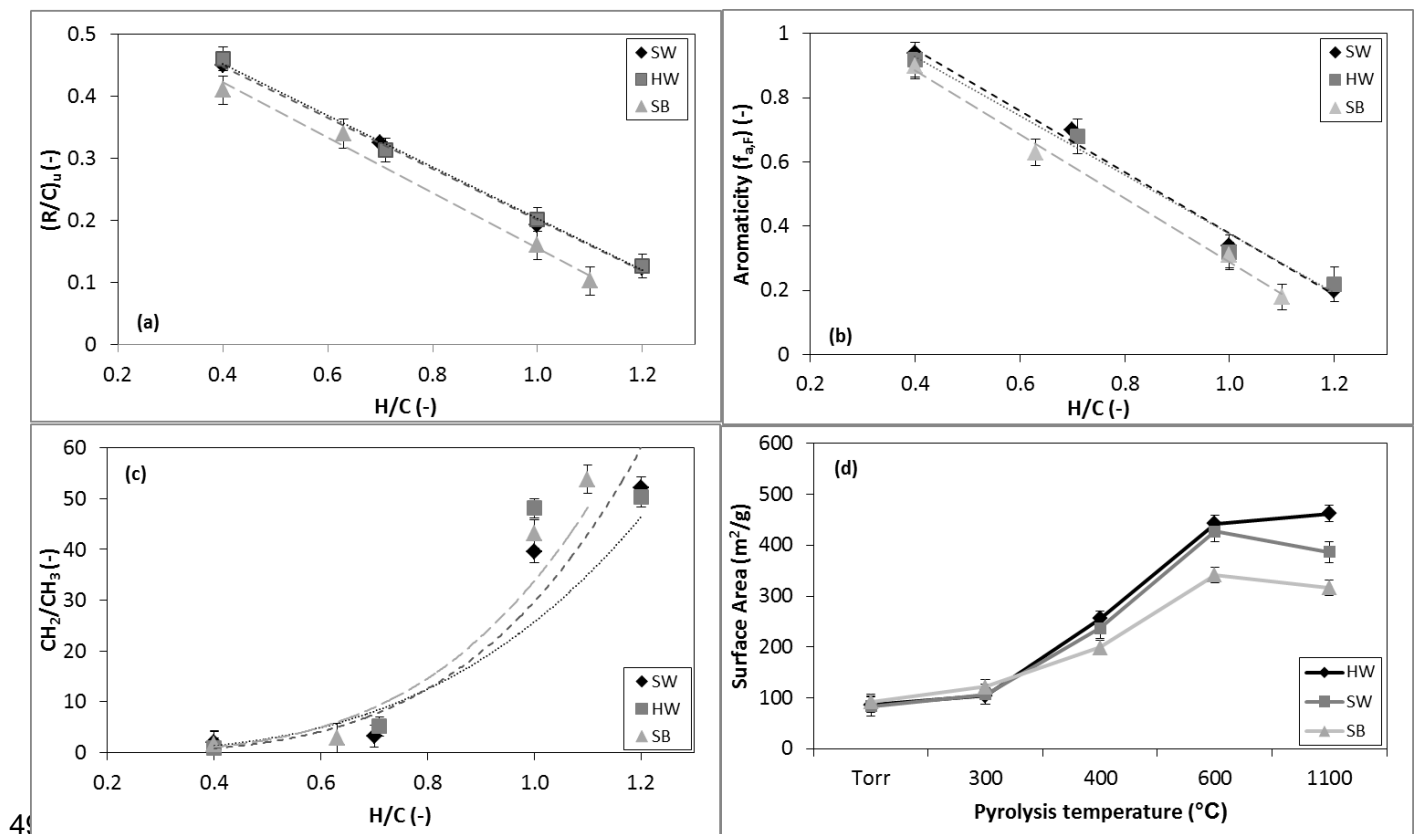
Figure 3: Correlations between the chemical characteristics of biomass and biomass chars.

502 **Table captions**

503 **Table 1:** Proximate and ultimate analyses for torrefied biomass and chars prepared at
504 different temperatures.

505 **Table 2:** Chemical parameters for torrefied biomass and chars.

506 **Table 3:** Structural characteristics of torrefied biomass and subsequent chars.

507 **Table 4**: Correlation equations of some properties of torrefied biomass and chars.

508

509 **Table 1:** Proximate and ultimate analyses for torrefied biomass and chars prepared at
510 different temperatures

Sample		VM[1]	FC[2]	Ash	CV[3] (MJ/kg)	C	H	N	S	O	H/C	O/C
		Proximate Analysis (wt.%, mfb)				**Ultimate Analysis (wt.%, daf)**						
SW	Torr	76.5	22.9	0.6	22.3	55.1	5.6	0.13	0.09	39.1	1.2	0.5
	300 °C	63.8	35.5	0.7	23.2	65.2	5.2	nd[4]	0.07	29.7	1.0	0.3
	400 °C	30.7	68.5	0.8	28.8	78.9	4.3	nd	0.06	16.7	0.7	0.2
	600 °C	9.9	89.2	1.0	33.1	95.7	2.9	0.08	0.07	1.2	0.4	0.01
	1100 °C	1.3	97.4	1.2	32.3	99.2	0.6	0.02	0.07	0.06	0.1	0.01
HW	Torr	77.3	22.1	0.6	22.4	55.4	5.4	0.01	0.03	39.2	1.2	0.5
	300 °C	64.2	35.3	0.6	23.2	61.2	5.1	nd	0.05	33.7	1.1	0.4
	400 °C	30.4	68.9	0.7	28.1	77.2	3.9	nd	0.04	18.8	0.6	0.2
	600 °C	10.1	89.2	0.8	33.7	93.4	3.0	nd	0.05	3.6	0.4	0.03
	1100 °C	1.2	97.5	1.2	32.1	99.2	0.7	0.03	0.04	0.03	0.1	0.01
SB	Torr	69.8	23.7	6.5	23.0	53.4	5.5	0.32	0.15	41.1	1.1	0.6
	300 °C	48.1	45.0	6.8	24.5	69.2	5.0	nd	0.16	25.1	1.0	0.3
	400 °C	26.2	66.1	7.6	26.6	77.9	4.3	0.11	0.15	17.6	0.7	0.2
	600 °C	5.8	82.0	12.2	30.1	92.2	3.1	0.36	0.19	4.2	0.4	0.03
	1100 °C	3.2	83.9	12.5	26.6	97.1	1.3	0.39	0.18	1.0	0.2	0.03

511 [1]VM - volatile matter, [2]FC - fixed carbon and [3]CV - calorific value, [4]nd - not detected

512

513   **Table 2:** Chemical parameters for torrefied biomass and chars.

Sample		Chemical Characteristics			
		$f_{a,N}$	$f_{a,F}$	$(R/C)_u$	CH_2/CH_3 ratio
SW	Torr	0.21	0.26	0.12	52.1
	300 °C	0.34	0.37	0.19	39.5
	400 °C	0.71	0.74	0.30	3.2
	600 °C	0.94	0.93	0.48	1.9
	1100 °C	-	-	-	-
HW	Torr	0.22	0.24	0.13	50.3
	300 °C	0.32	0.30	0.20	48.1
	400 °C	0.68	0.62	0.31	5.2
	600 °C	0.92	0.92	0.46	1.0
	1100 °C	-	-	-	-
SB	Torr	0.18	0.23	0.10	53.8
	300 °C	0.31	0.47	0.16	43.1
	400 °C	0.63	0.63	0.34	2.9
	600 °C	0.90	0.96	0.41	1.6
	1100 °C	-	-	-	-

514

515

516

517

518

519

520

521

522

523

524

525

526

527

528

529

21

530   **Table 3:** Structural characteristics of torrefied biomass and subsequent chars.

Sample ID		CO_2 adsorption			WA-XRD-CFA				
		S.A (m^2/g)	M.P.V (cm^3/g)	M.P.W (Å)	d_{002} (Å)	L_c (Å)	L_a (Å)	N_{ave} (-)	X_a (-)
SW	Torr	83	0.017	3.7	4.0	27	72.0	7.8	0.34
	300 °C	107	0.022	3.6	4.1	19	74	5.6	0.42
	400 °C	236	0.055	3.8	3.9	10	86	3.7	0.21
	600 °C	427	0.092	3.9	3.8	10	125	3.6	0.08
	1100 °C	386	0.083	4.4	3.7	9	139	3.5	-
HW	Torr	86	0.018	3.7	4.0	30	65	8.5	0.35
	300 °C	103	0.022	3.6	4.0	17	67	5.2	0.41
	400 °C	255	0.059	3.7	3.9	12	85	4.0	0.18
	600 °C	442	0.094	3.8	3.8	10	115	3.7	0.07
	1100 °C	461	0.097	4.0	3.8	9	130	3.5	-
SB	Torr	92	0.02	3.7	4.1	28	69	8.0	0.34
	300 °C	121	0.026	3.6	4.2	17	71	5.0	0.15
	400 °C	198	0.049	3.5	4.0	13	89	4.3	0.06
	600 °C	341	0.073	3.6	3.9	12	135	4.0	-
	1100 °C	316	0.072	3.9	3.8	10	151	3.6	-

531

532

533

534

535

536

537

538

539

540

541

542

22

543   **Table 4:** Correlation equations of some properties of torrefied biomass and subsequent chars.

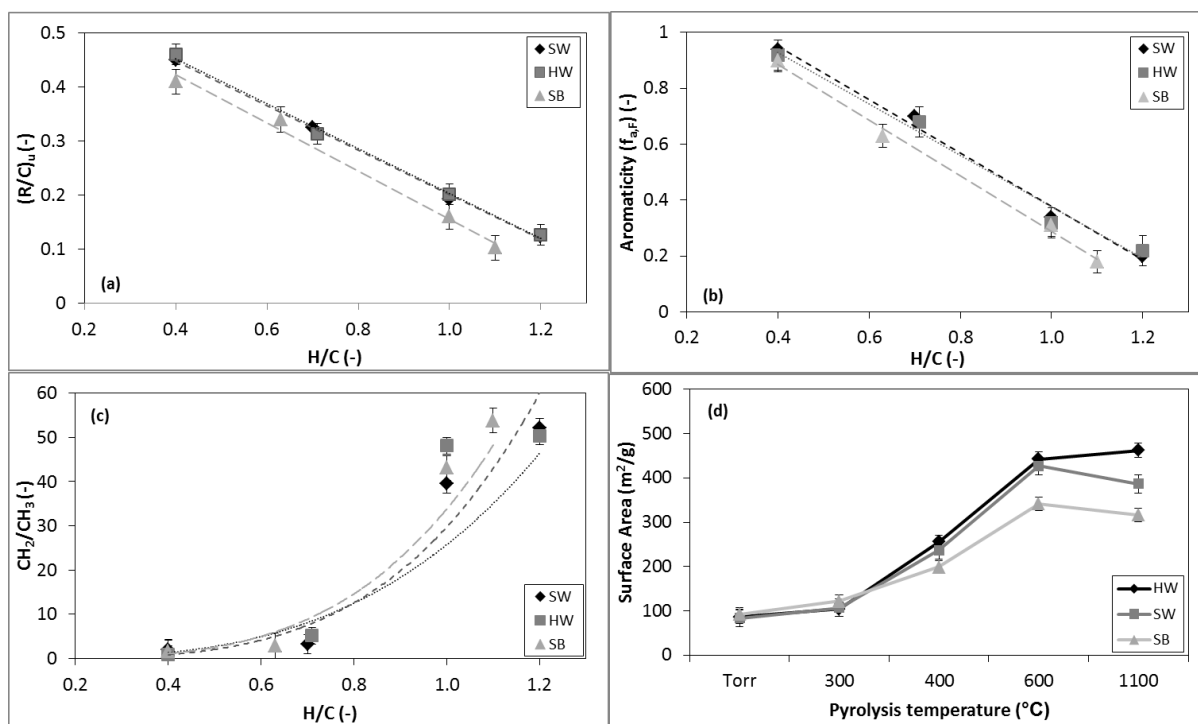| Parameter	Sample ID	Correlation equation	R^2
$f_{a,F}$	SW	$f_{a,F} = -0.96(H/C) + 1.34$	0.991
	HW	$f_{a,F} = -0.92(H/C) + 1.30$	0.983
	SB	$f_{a,F} = -0.99(H/C) + 1.28$	0.995
$(R/C)_n$	SW	$(R/C)_n = -0.41(H/C) + 0.61$	0.998
	HW	$(R/C)_n = -0.42(H/C) + 0.62$	0.997
	SB	$(R/C)_n = -0.44(H/C) + 0.60$	0.990
CH_2/CH_3	SW	$CH_2/CH_3 = 26(H/C)^{3.23}$	0.858
	HW	$CH_2/CH_3 = 29.8(H/C)^{3.85}$	0.958
	SB	$CH_2/CH_3 = 33.8(H/C)^{3.74}$	0.924

544

545

546

547

548

549

550

551 **Highlights**

552 • Lignocellulosic biomass pyrolysis is a 2-step process

553 • Aromaticity can be determined from ATR-FTIR spectroscopy

554 • Aliphatic chains decrease with increasing pyrolysis temperature

555 • The carbon lattice is stretchered into sheets as temperature is increased

556